UAV-Based 3D Spectrum Sensing in Spectrum-Heterogeneous Networks

Feng Shen, Guoru Ding, *Senior Member, IEEE*, Zheng Wang, *Member, IEEE*, and Qihui Wu, *Senior Member, IEEE*

***Abstract*—In cognitive radio networks, collaborative spectrum sensing has been recognized as a key technology to enable secondary users (SUs) to detect spectrum holes and opportunistically access primary licensed spectrum band without harmful interference. Most of the existing studies focus on 1D or 2D spectrum opportunity detection and explicitly or implicitly assume that all SUs share the same spectrum opportunity. In this paper, we first investigate the issue of joint spatial-temporal spectrum sensing in 3D spectrum-heterogeneous space by leveraging the location flexibility of flying unmanned aerial vehicle (UAV) spectrum sensors. We divide the sensing space into three layers: *black layer*, *grey layer*, and *white layer*, which represent different spatial spectrum access opportunities. Then, we formulate the 3D spatial-temporal opportunity sensing model and derive the spatial-temporal false alarm and detection probabilities at both single UAV level and whole network level. Afterwards, we design a temporal fusion window and a spatial fusion sphere to address the composite spatial-temporal data fusion, called 3D spatial-temporal sensing (3DSTS). A comparison among 3DSTS, the benchmark 3D non-cooperative sensing (3DNCS) and 3D cooperative sensing (3DCS) shows the inefficiency of the traditional sensing schemes in the 3D spectrum-heterogeneous networks. Furthermore, we develop three improved versions of 3DSTS, which show much better detection performance. To maximize the utilization of spectrum resource and minimize the interference to the PU, a sensing-based power control scheme is also proposed. Finally, numerical simulations corresponding to the theoretical analysis are demonstrated.**

***Index Terms*—Spectrum sensing, cognitive radio network, unmanned aerial vehicles, spectrum-heterogeneity.**

Manuscript received July 11, 2018; revised November 5, 2018 and February 4, 2019; accepted March 12, 2019. Date of publication April 3, 2019; date of current version June 18, 2019. This work was supported in part by the National Natural Science Foundation of China under Grants 61501510, 61631020, and 61801216, in part by the Fundamental Research Funds for the Central Universities under Grants NP2018103, NE2017103, and NC2017003, in part by the Research Funds of State Key Laboratory of Complex Electromagnetic Environment Effects on Electronics and Information System under Grant CEMEE2018K0103B, in part by the China Postdoctoral Science Foundation Funded Project under Grant 2018T110426, and in part by the Natural Science Foundation of Jiangsu Province under Grant BK20180420. The review of this paper was coordinated by Dr. K. Bian. *(Corresponding author: Zheng Wang.)*

F. Shen, Z. Wang, and Q. Wu are with the College of Electronics and Information Engineering, Nanjing University of Aeronautics and Astronautics, Nanjing 211106, China (e-mail: sfjx_nuaa@163.com; z.wang@ieee.org; wuqihui2014@sina.com).

G. Ding is with the College of Communications Engineering, Army Engineering University, Nanjing 210007, China, and also with the National Mobile Communications Research Laboratory, Southeast University, Nanjing 210018, China (e-mail: dr.guoru.ding@ieee.org).

Digital Object Identifier 10.1109/TVT.2019.2909167

I. Introduction

A. Background and Motivation

With the explosion of wireless devices and services, the contradiction between the increasingly crowded spectrum and the underutilization of spectrum resources is becoming more and more acute [1]. The studies by the Federal Communications Commission (FCC) indicate that some unlicensed bands such as industrial, scientific, medical bands and licensed bands for land mobile communications are overcrowded [2], [3], however, most of licensed bands allocated to for example broadcasting TVs or military radars are often used inefficiently. Therefore, if the system can automatically perceive the spectrum environment, adjust or adapt the transmission parameters in real time through intelligent learning, and occupy the idle frequency bands which are licensed to the primary user to realize the opportunistic access of the space spectrum, then the spectrum utilization will be undoubtedly improved [4]. Consequently, the revolutionary spectrum sharing technology, cognitive radio (CR) [5]–[8] comes out, which is thought to be an effective solution to this contradiction. Spectrum sensing is an important part of cognitive radio. Only by adopting a suitable spectrum detection strategy for the corresponding wireless communication environment, can the secondary user (SU) detect the spectrum occupancy states with a high detection probability and thereby make a correct decision whether to access the frequency band or not [9]–[13].

Most of existing studies focus on either temporal or spatial spectrum sensing in 1D or 2D spectrum space and assume that all the SUs share the same opportunity to occupy the licensed channel. Recently, the increasing popularity of UAVs in both civil and military fields has been witnessed [14]–[16], which on one hand, results in new demand of spectrum resources, while on the other hand, poses promising potentials to explore and exploit spectrum opportunity in 3D spectrum space by properly leveraging the location flexibility of flying UAV spectrum sensors. These observations motivate us in this paper to consider how to define and efficiently exploit the 3D spectrum opportunity by developing a joint spatial-temporal sensing scheme in spectrum-heterogeneous networks based on UAVs.

B. Related Work

Majority of existing studies on spectrum sensing can be divided into three groups: temporal spectrum sensing, spatial spectrum sensing and spatial-temporal spectrum sensing. As for

temporal spectrum sensing, it is usually modeled as a binary hypothesis testing between the presence and absence of a primary signal [17]–[19]. Multiuser diversity is further exploited, which shows cooperative sensing (CS) can achieve better detection performance than non-cooperative sensing (NCS)(see, e.g., [20]–[22]).

Research results on spatial spectrum sensing are relatively limited. In [23]–[25], the authors estimate the location and transmission power of PU and also show how spatial correlation impacts the overall performance. Nevertheless, they don't take the spatial heterogeneity into consideration. The studies in [26], [27] model the problem of spatial spectrum-heterogeneous sensing and present the spatial false alarm issue. The studies in [28], [29] creatively execute cooperative spectrum sensing in heterogeneous cognitive radio networks via Belief Propagation and Bayesian Clustering, respectively.

There are also some related studies on spatial-temporal spectrum sensing. In [30], the authors study the performance of joint spatial-temporal spectrum sensing. The relationship between spatial spectrum sensing and temporal spectrum sensing with constrained interference on primary user is investigated. An optimization problem is also formulated to maximize the throughput of secondary system in CRNs. In [31], the authors also propose a joint spatial-temporal sensing scheme, which exploits information from spatial sensing to improve the performance of temporal sensing. Moreover, in the spatial sensing, SU information is chosen intelligently based on the SU location towards PU to minimize the correlation. In [32], the authors use the weighted centroid algorithm to localize the position of the PU. Then they adopt a selective measurement combining for weighted average consensus to fuse detection results of homogeneous sensor nodes. In our prior work [33], we manage to design a two-dimensional sensing (TDS) framework to execute spatial-temporal opportunity detection in spectrum-heterogeneous cognitive radio networks, which exploits correlations in time and space simultaneously by effectively fusing sensing results in a spatial-temporal sensing window.

It is observed that although the topic of spectrum sensing has been extensively studied, to the best of the authors' knowledge, most of existing studies focus on either temporal or spatial spectrum sensing in 1D or 2D spectrum space and assume that all the SUs share the same opportunity to occupy the licensed channel, there are no reports on 3D spectrum opportunity exploitation in spectrum-heterogeneous environment, which will be studied in this paper.

C. Contributions

The main contributions of this paper are summarized as follows:

- By leveraging the location flexibility of flying UAV spectrum sensors, we define the 3D spatial-temporal spectrum opportunity and model the 3D spatial-temporal sensing process as a composite hypothesis testing problem, based on which, we derive the closed-form expressions of the spatial-temporal false alarm probability and detection probability at both single UAV level and whole network level.
- We develop a 3D spatial-temporal sensing (3DSTS) framework for opportunity detection in spectrum-heterogeneous environment based on UAVs. We design a temporal window and a spatial sphere to execute spatial-temporal data fusion, which helps to exploit the temporal and spatial correlations in the sensing results. Simulation results show that 3DSTS can overcome the weakness of the benchmark 3DNCS and 3DCS, and provide an efficient sensing framework for spectrum-heterogeneous networks.
- We propose three new sensing schemes to improve the 3DSTS scheme. They are called double fusion 3DSTS (DF-3DSTS), temporal and global spatial sensing (TGSS) and double fusion temporal and global spatial sensing (DF-TGSS). Comparisons show these schemes achieve much better detection performance. We also study the impact of different parameters (PU sensed range R_s, PU working probability P_1, UAV density ρ and NLOS channel) on the detection performance, thus we are able to choose the best sensing method in different spectrum environment.
- We propose a sensing based power control scheme to make full use of the spectrum resource with maximum constrained interference. It can effectively exploit spectrum opportunities of the *grey layer* in spectrum-heterogeneous networks, thus achieving much higher spectrum utilization.

The remainder of this paper is organized as follows. In Section II, the system model and problem of interest are introduced. Then, the performance metrics and performance analysis are presented in Section III. The 3D spatial-temporal sensing framework and three improved sensing algorithms based on 3DSTS in spectrum-heterogeneous networks are proposed in Section IV. In Section V, a sensing based power control scheme is discussed. Section VI presents the simulation results and Section VII draws conclusions.

II. System Model and Problem Formulation

A. 3D Spectrum-Heterogeneous Network Model

In this paper, we consider a cognitive radio network as shown in Fig. 1, in which a TV tower locates at the center of the hemisphere and $|N|$ UAVs randomly distribute in the hemisphere area, obeying a 3D Poisson Process [34]. The PU transmission region with a radius R_p is called *black layer*, which means the maximum distance that the primary receiver can receive the primary signal. If a UAV occupies the TV band inside R_p, it will definitely block the normal communication of the licensed users on the ground or in the tall buildings. The *white layer* has a radius R_s, which is called PU sensed range. Any UAV beyond R_s cannot detect the primary signal anymore. However, even if a UAV lies outside the PU transmission region, its spectrum occupancy may still cause harmful interference to primary receivers, depending on how close the UAV is to the PU and how much transmission power it uses. Therefore, we design a transition layer between *black layer* and *white layer* called *grey layer* with a radius R_{pp}, in which a power control scheme will be applied to improve spectrum utilization and also avoid harmful interference to PU. The sphere with a radius R_g in Fig. 1 is called fusion sphere. It assists the UAV at the sphere center to make decisions with the help of its neighbor UAVs inside the fusion sphere.

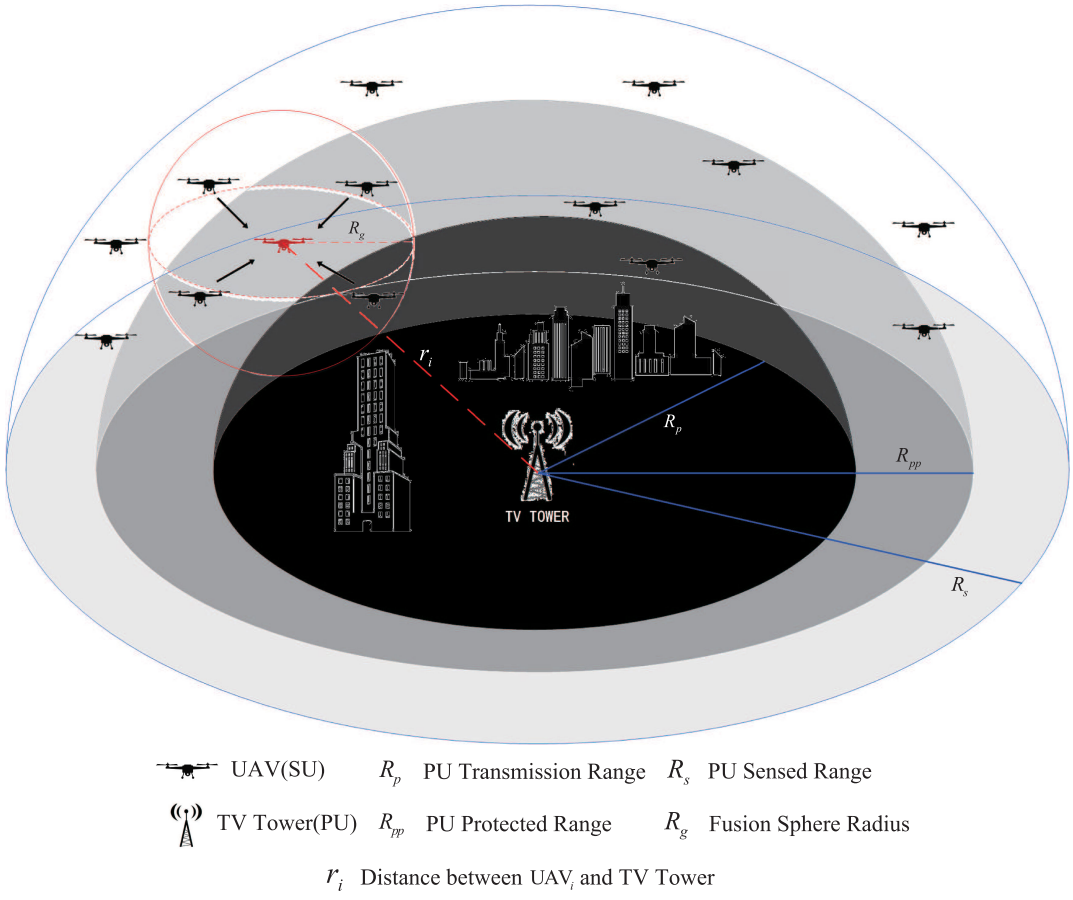

Fig. 1. System model. The hemisphere around TV tower is divided into *black-grey-white* three layers. The *black layer* with a radius R_p is called PU transmission region. The *white layer* has a radius R_s, which is called PU sensed range. The transition *grey layer* has a radius R_{pp}. The sphere with a radius R_g is called fusion sphere, it assists the UAV to make decisions with the help of its neighbor UAVs. Based on this *black-grey-white* network model, we design a 3D spatial-temporal sensing framework and execute 3D spatial-temporal opportunity detection.

Based on this *black-grey-white* network model, we will formulate the 3D spatial-temporal opportunity detection process and design a 3D spatial-temporal sensing framework thereinafter.

B. Composite Spatial-Temporal Opportunity Model

Most traditional detection schemes only take time domain into consideration, which turns out to be a binary hypothesis testing problem [17]:

$$\begin{cases} H_0 : x_i(n) = n_i(n), n = 1, \ldots, M, \\ H_1 : x_i(n) = \sqrt{P_i(r_i)} s_i(n) + n_i(n), n = 1, \ldots, M, \end{cases} \tag{1}$$

where M is the total sample number, $x_i(n)$ represents the nth received sampling signal by the ith UAV, $n_i(n)$ is the additive white Gaussian noise with variance ${\sigma_n}^2$ and $s_i(n)$ is the PU transmission signal. $P_i(r_i)$ is the attenuated received PU signal at the ith UAV with a distance r_i from PU.

Similarly, from the spatial view, another binary hypothesis testing is widely used [27]:

$$\begin{cases} S_0 : R_{pp} \le r_i \le R_s, \\ S_1 : 0 \le r_i \le R_{pp}, \end{cases} \tag{2}$$

where r_i represents the distance between the ith UAV and PU. If the distance r_i is smaller than R_{pp}, then it is pure temporal spectrum sensing in the homogeneous *black layer*. If the distance is between R_{pp} and R_s, the UAV's spectrum occupancy will have no interference on the TV tower. Most studies usually take only black or white opportunity into consideration as Eq.(2) shows, however, we will consider spatial opportunity in the *grey layer*, i.e., to distinguish between black, grey and white opportunities.

In order to improve the spectrum utilization and lower the receiver's spectrum sensing sensitivity requirement, we will first simplify the spatial sensing model to two layers. We replace the PU protected range R_{pp} with the PU transmission range R_p (i.e., treat the *grey layer* as a part of *white layer*). In this way, not only is the utilization of available spectrum improved, but also it helps to design the power control scheme of the *grey layer* later in Section V.

Based on the above temporal and spatial hypothesis testing formulations, we define the composite spatial-temporal opportunity detection model as follows:

$$\begin{cases} O_0 : H_0 \cup S_0, \\ O_1 : H_1 \cap S_1, \end{cases} \tag{3}$$

where $O_0 = H_0 \cup S_0$ denotes the UAV has a spatial-temporal opportunity, either because the working state of PU is OFF (H_0) or the SU is located outside the PU transmission range (S_0). $O_1 = H_1 \cap S_1$ represents the SU is located inside the PU transmission range (S_1) and the working state of PU is ON (H_1)

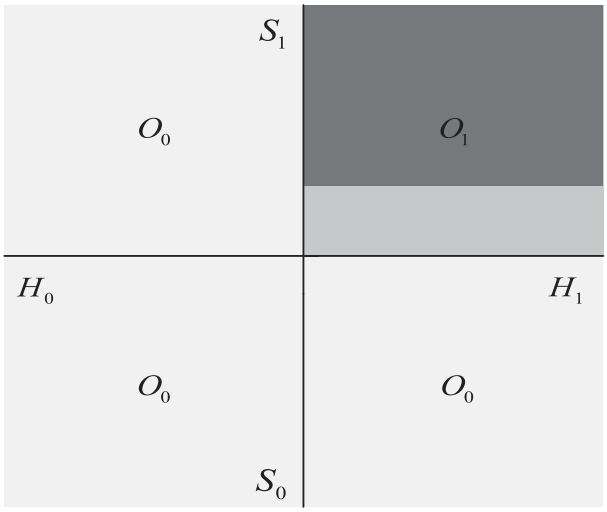

Fig. 2. Composite spatial-temporal opportunity model. The black, grey, and white blocks represent different spatial-temporal spectrum opportunities in *black*, *grey*, and *white layers*. It can be regarded as a binary decision between the first quadrant (O_1) and the second-third-fourth quadrants (O_0), $O_0 = H_0 \cup S_0$, $O_1 = H_1 \cap S_1$.

at the same time. These formulations are illustrated as Fig. 2 shows.

Substituting formulas (1) and (2) into (3), we get

$$\begin{cases} O_0 : x_i(n) = \begin{cases} n_i(n), 0 \le r_i \le R_s, \\ \sqrt{P_i(r_i)} s_i(n) + n_i(n), R_p \le r_i \le R_s, \end{cases} \\ O_1 : x_i(n) = \sqrt{P_i(r_i)} s_i(n) + n_i(n), 0 \le r_i \le R_p. \end{cases} \tag{4}$$

III. Performance Metrics and Analysis

A. Composite Spatial-Temporal Opportunity Detection Performance Metrics

In this paper, we evaluate the detection performance by false alarm probability and detection probability at single UAV level and whole network level [33], [35]. According to (4), we define the spatial-temporal false alarm probability $P_{f,i}^{ST}(k)$ and detection probability $P_{d,i}^{ST}(k)$ as follows,

$$P_{f,i}^{ST}(k) = P(O_1|O_0), \tag{5}$$

$$P_{d,i}^{ST}(k) = P(O_1|O_1), \tag{6}$$

where k denotes the kth sensing period, i denotes the ith UAV in the network. Furthermore, we define the network spatial-temporal false alarm probability and detection probability as:

$$P_{f,net}^{ST} = \frac{1}{|T| \cdot |N|} \sum_{k \in T} \sum_{i \in N} P_{f,i}^{ST}(k), \tag{7}$$

$$P_{d,net}^{ST} = \frac{1}{|T| \cdot |N_{in}|} \sum_{k \in T} \sum_{i \in N_{in}} P_{d,i}^{ST}(k), \tag{8}$$

where T denotes the set of consecutive sensing periods, N denotes the set of all UAVs in the network and N_{in} represents the set of UAVs inside the TV tower transmission range. $|\cdot|$ denotes the size of the set.

B. 3D Non-Cooperative Sensing and 3D Cooperative Sensing in Spectrum-Heterogeneous Networks

For each UAV, we consider energy detection as the means of signal detection which is a simple and effective method. The test statistic for energy-based opportunity detection by each UAV is:

$$E_i(k) = \frac{1}{M} \sum_{n=1}^{M} [x_i(n)]^2. \tag{9}$$

According to the central limit theorem (CLT), when the sample number is sufficiently large (e.g., $M \gg 10$), $E_i(k)$ is approximated as a Gaussian random variable under both hypotheses H_0 and H_1 in the kth sensing period [36], [37].

$$E_i(k) \sim \begin{cases} \mathcal{N}(\mu_0, {\sigma_0}^2), & H_0 \\ \mathcal{N}(\mu_1(r_i), {\sigma_1}^2(r_i)), & H_1 \end{cases} \tag{10}$$

where

$$\begin{cases} \mu_0 = {\sigma_n}^2, \\ {\sigma_0}^2 = 2{\sigma_n}^4/M, \\ \mu_1(r_i) = (1+\gamma_i){\sigma_n}^2 = (1+\gamma_i)\mu_0, \\ {\sigma_1}^2(r_i) = 2(1+2\gamma_i){\sigma_n}^4/M = (1+2\gamma_i){\sigma_0}^2, \end{cases} \tag{11}$$

$\gamma_i = P_i(r_i)/{\sigma_n}^2$ represents the received signal to noise ratio (SNR) of the ith UAV. As for 3D non-cooperative sensing (3DNCS), we have $E_{3DNCS} = E_i(k)$, $\mu_{3DNCS,0} = \mu_0$, ${\sigma_{3DNCS,0}}^2 = {\sigma_0}^2$, $\mu_{3DNCS,1}(r_i) = \mu_1(r_i)$, ${\sigma_{3DNCS,1}}^2(r_i) = {\sigma_1}^2(r_i)$.

Based on the above approximate distribution, we can get the spatial-temporal false alarm probability and detection probability for each UAV (i.e., 3DNCS).

$$P_{f,i}^{ST}(k) = \begin{cases} P_{f,i}^{T_0}(k), & 0 \le r_i \le R_p, \\ (1-P_1)P_{f,i}^{T_0}(k) + P_1 P_{f,i}^{T_1}(k), & R_p \le r_i \le R_s, \end{cases}$$

$$= \begin{cases} Q\left(\frac{\lambda - \mu_{3DNCS,0}}{\sigma_{3DNCS,0}}\right), & 0 \le r_i \le R_p, \\ (1-P_1)Q\left(\frac{\lambda - \mu_{3DNCS,0}}{\sigma_{3DNCS,0}}\right) \\ \quad + P_1 Q\left(\frac{\lambda - \mu_{3DNCS,1}(r_i)}{\sigma_{3DNCS,1}(r_i)}\right), & R_p \le r_i \le R_s, \end{cases} \tag{12}$$

$$P_{d,i}^{ST}(k) = P_{d,i}^{T_1}(k), \quad 0 \le r_i \le R_p,$$

$$= Q\left(\frac{\lambda - \mu_{3DNCS,1}(r_i)}{\sigma_{3DNCS,1}(r_i)}\right), \quad 0 \le r_i \le R_p, \tag{13}$$

where λ represents decision threshold to distinguish O_0 and O_1. P_1 represents the probability that the TV tower is working. $P_{f,i}^{T_0}(k)$ and $P_{d,i}^{T_1}(k)$ are pure temporal false alarm probability and detection probability for the ith UAV in the kth sensing period, respectively. The superscript T_0 and T_1 represent the temporal absence (H_0) and presence (H_1) of the PU signal, respectively. We can find that the joint spatial-temporal false alarm probability is divided into two situations. One is when the UAV is located in the *black layer* ($r_i \le R_p$), the false alarm probability is same as the traditional temporal hypothesis testing problem; the other is when UAV is located in the *grey* or *white layers* ($R_p < r_i \le R_s$), the false alarm probability at this time can further be divided into two cases: one is that the TV tower is OFF,

but the detection result indicates that it is occupying the spectrum; the other is that the TV tower is ON, the detection result indicates that the it is occupying the spectrum. Actually, regardless of TV tower's working state, UAV located in the *grey* or *white layers* ($R_p < r_i \leq R_s$) can occupy spectrum freely, without affecting the TV tower.

Note that, when the UAV is located in the *grey* or *white layer*, the spatial spectrum access opportunity we get is essentially temporal opportunity. Because when the UAV is outside the transmission range of the TV tower, no matter whether the TV tower is working or not, the false alarm occurs because the UAV mistakenly believes that the TV tower is working and does not occupy the spectrum in order to prevent interference.

Furthermore, we derive the network false alarm probability and detection probability of the 3DNCS in the spectrum-heterogeneous networks,

$$P_{f,net}^{ST} = \frac{1}{|N|}\left\{ \sum_{i\in N_{in}} Q\left(\frac{\lambda-\mu_{3DNCS,0}}{\sigma_{3DNCS,0}}\right) + \sum_{i\in N_{out}} \left[(1-P_1)\times Q\left(\frac{\lambda-\mu_{3DNCS,0}}{\sigma_{3DNCS,0}}\right) + P_1 Q\left(\frac{\lambda-\mu_{3DNCS,1}(r_i)}{\sigma_{3DNCS,1}(r_i)}\right)\right]\right\}, \tag{14}$$

$$P_{d,net}^{ST} = \frac{1}{|N_{in}|}\sum_{i\in N_{in}} Q\left(\frac{\lambda-\mu_{3DNCS,1}(r_i)}{\sigma_{3DNCS,1}(r_i)}\right), \tag{15}$$

where N_{in} and N_{out} denote the set of UAVs located inside and outside the TV tower transmission range, respectively.

Similarly, we consider the 3D cooperative sensing (3DCS) detection performance in 3D spectrum-heterogeneous networks. The 3DCS test statistic is a linearly weighted combination of the observed energy values from all UAVs $E_{3DCS} = \sum_{i=1}^{|N|} \omega_i E_i$, where E_i is the observed energy of the ith UAV. ω_i is the weight coefficient of the ith UAV in the cooperative sensing scheme [17], defined as

$$\omega_i = \frac{SNR_i}{\sqrt{\sum_{k=1}^{|N|} SNR_k}}, \tag{16}$$

where SNR_i is the received signal to noise ratio at the ith UAV. Therefore, the distribution of the cooperative sensing test statistic follows

$$E_{3DCS} \sim \begin{cases} \mathcal{N}(\mu_{3DCS,0}, {\sigma_{3DCS,0}}^2), & H_0 \\ \mathcal{N}(\mu_{3DCS,1}(r_i), {\sigma_{3DCS,1}}^2(r_i)), & H_1 \end{cases} \tag{17}$$

where

$$\begin{cases} \mu_{3DCS,0} = \sum_{i=1}^{|N|} \omega_i {\sigma_n}^2, \\ {\sigma_{3DCS,0}}^2 = \sum_{i=1}^{|N|} 2\omega_i^2 {\sigma_n}^4/M, \\ \mu_{3DCS,1}(r_i) = \sum_{i=1}^{|N|} (1+\gamma_i)\omega_i {\sigma_n}^2, \\ {\sigma_{3DCS,1}}^2(r_i) = \sum_{i=1}^{|N|} \omega_i^2 (1+2\gamma_i){\sigma_0}^2, \end{cases} \tag{18}$$

$\gamma_i = P_i(r_i)/{\sigma_n}^2$ represents the received signal to noise ratio (SNR) of the ith UAV.

Based on the above approximate distribution of 3DNCS scheme and equations (12), (13), (14) and (15), we can easily obtain the 3DCS spatial-temporal false alarm probability and detection probability of single UAV and whole network.

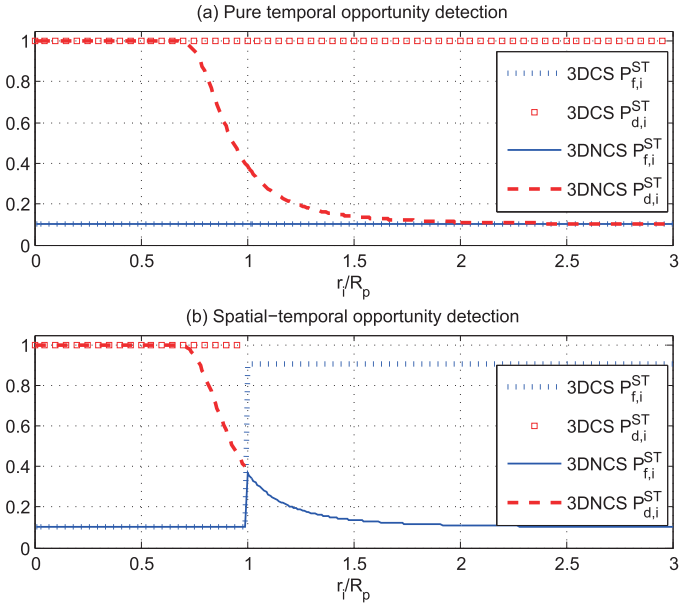

Fig. 3. Pure temporal and spatial-temporal detection performance comparisons between 3DNCS and 3DCS for a single UAV. $P_1 = 0.9$, the pure temporal false alarm probability $P_{f,i}^{T_0} = 0.1$.

$$P_{f,i}^{ST}(k) = \begin{cases} P_{f,i}^{T_0}(k), & 0 \leq r_i \leq R_p, \\ (1-P_1)P_{f,i}^{T_0}(k) + P_1 P_{d,i}^{T_1}(k), & R_p \leq r_i \leq R_s, \end{cases}$$

$$= \begin{cases} Q\left(\frac{\lambda-\mu_{3DCS,0}}{\sigma_{3DCS,0}}\right), & 0 \leq r_i \leq R_p, \\ (1-P_1)Q\left(\frac{\lambda-\mu_{3DCS,0}}{\sigma_{3DCS,0}}\right) + P_1 Q\left(\frac{\lambda-\mu_{3DCS,1}(r_i)}{\sigma_{3DCS,1}(r_i)}\right), & R_p \leq r_i \leq R_s, \end{cases} \tag{19}$$

$$P_{d,i}^{ST}(k) = P_{d,i}^{T_1}(k), \quad 0 \leq r_i \leq R_p,$$
$$= Q\left(\frac{\lambda-\mu_{3DCS,1}(r_i)}{\sigma_{3DCS,1}(r_i)}\right), \quad 0 \leq r_i \leq R_p, \tag{20}$$

$$P_{f,net}^{ST} = \frac{1}{|N|}\left\{ \sum_{i\in N_{in}} Q\left(\frac{\lambda-\mu_{3DCS,0}}{\sigma_{3DCS,0}}\right) + \sum_{i\in N_{out}} \left[(1-P_1)Q\left(\frac{\lambda-\mu_{3DCS,0}}{\sigma_{3DCS,0}}\right) + P_1 Q\left(\frac{\lambda-\mu_{3DCS,1}(r_i)}{\sigma_{3DCS,1}(r_i)}\right)\right]\right\}, \tag{21}$$

$$P_{d,net}^{ST} = \frac{1}{|N_{in}|}\sum_{i\in N_{in}} Q\left(\frac{\lambda-\mu_{3DCS,1}(r_i)}{\sigma_{3DCS,1}(r_i)}\right). \tag{22}$$

According to the theoretical derivation of 3DNCS and 3DCS, we compare their detection performance for a single UAV in Fig. 3 with temporal false alarm probability $P_{f,i}^{T_0} = 0.1$. As Fig. 3(a) shows, the pure temporal detection probability of a UAV in 3DNCS decreases monotonically with distance r_i, mainly due to the reduced received SNR. However, the pure temporal detection probability of a UAV in 3DCS remains the same with the varying r_i, mainly due to the multiuser diversity [20]. On the

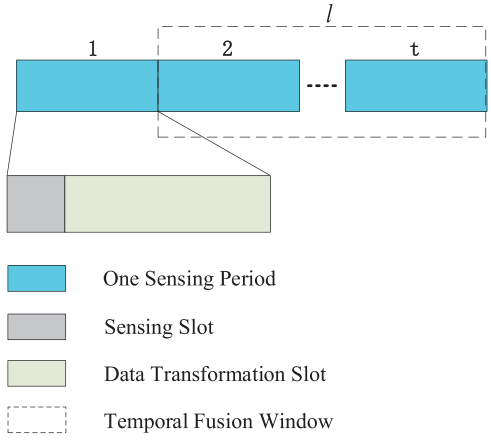

Fig. 4. Temporal fusion. A temporal fusion window is defined to combine multiple sensing results in successive sensing periods. The window length is denoted as l, from $t-l+1$ to t.

other hand, in Fig. 3(b), when the UAV is in homogeneous environment ($r_i \leq R_p$), the detection probability of 3DCS is higher than 3DNCS due to multiuser diversity which is same as the case of pure temporal detection. However, in the heterogeneous environment ($r_i > R_p$), the 3DCS scheme produces a much higher false alarm probability than 3DNCS mainly due to the high spatial false alarm probability introduced by cooperation [26].

IV. 3D Spatial-Temporal Sensing Framework

A. Composite Spatial-Temporal Data Fusion and Decision Making

For the inefficiency of the 3DNCS and 3DCS schemes in 3D spectrum-heterogeneous environment, we will introduce the 3D spatial-temporal sensing (3DSTS) and move on to derive its false alarm probability and detection probability from the perspective of single UAV and whole network, sequentially.

We are going to formulate the data fusion process and the final decision making of the TV tower's working state. Typically, spectrum sensing results have strong correlations in time domain and space domain. That is, the sensing result obtained in short time ago is usually the same as that of the current period, and two spatially close SUs generally have similar sensing results. The above fact guides us to exploit both temporal and spatial correlations in spectrum sensing of spectrum-heterogeneous networks.

Firstly, we consider the temporal fusion, as shown in Fig. 4. The entire time is divided into many successive sensing periods, and each sensing period is divided into two parts: the sensing slot and the transmission slot. In the sensing slot, the UAV senses the spectrum environment and detects whether the PU is working. If the PU is detected to be idle, the UAV will occupy the spectrum in the transmission slot for data transmission. In order to exploit the temporal correlation, we define a temporal fusion window, it combines multiple sensing results in successive sensing periods. The window length is decided by the minimum number of sensing periods that hold the same primary user state. We denote the window length $l = min(1/(\varepsilon T_p), 1/(\mu T_p)$, where ε(times/ms) and μ(times/ms) are transition rates of the PU state from OFF to ON and from ON to OFF. T_p is the duration of each sensing

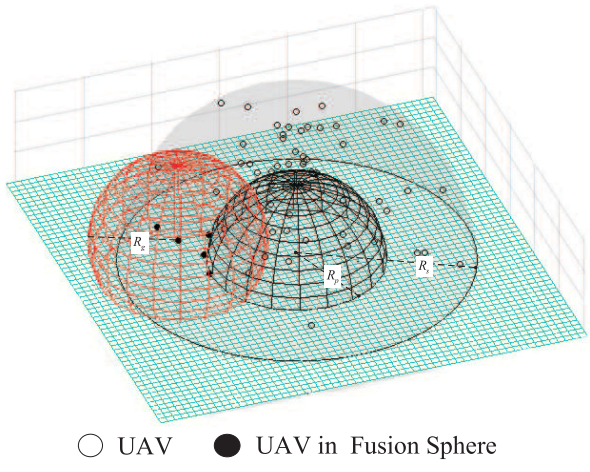

Fig. 5. Spatial fusion. The red sphere is defined as a spatial fusion sphere S with a radius R_g, the black dots and white dots are UAVs inside and outside the spatial fusion sphere, respectively. The black UAV at the center of the fusion sphere exchange sensing results with all the other UAVs located in its spatial fusion sphere.

period. Thus, the temporal fusion of the sensing period t can be obtained by linearly fusing the sensing results in the temporal fusion window, i.e.,

$$\hat{T}_i(t) = \sum_{k=t-l+1}^{t} \omega_k E_i(k), i = 1, \ldots, |N|, \tag{23}$$

where $E_i(k)$ is the ith sensing result of SU in the kth sensing period, index k ranges from $t-l+1$ to t. ω_k is the normalized temporal correlation weight coefficient in the kth sensing period defined as

$$\omega_k = \frac{\varphi_k}{\sum_{u=t-l+1}^{t} \varphi_u}, \tag{24}$$

where $\varphi_k = e^{-\tau_0(t-k)}$ denotes the temporal correlation between the current and historical sensing results, τ_0 is a positive adjustable parameter.

Then, each UAV executes spatial fusion. As shown in Fig. 5, we define a spatial fusion sphere (the red sphere, denoted as S) which is centered at the ith UAV with a radius R_g. The ith UAV will exchange sensing results with all the other UAVs which are located in the spatial fusion sphere and named as neighbor UAVs set. Similar to temporal fusion, we linearly fuse the sensing results of each UAV in the sphere,

$$T_i(t) = \sum_{j \in S} \rho_j \hat{T}_j(t), i = 1, \ldots, |N|, \tag{25}$$

where $\hat{T}_j(t)$ is the temporal fusion result of the jth neighbor UAV of the ith UAV in the spatial fusion sphere S. ρ_j is the normalized spatial correlation weight coefficient of the jth neighbor of the ith UAV, defined as

$$\rho_j = \frac{\phi_j}{\sum_{v \in S} \phi_v}, \tag{26}$$

where ϕ_j denotes the spatial correlation between the ith UAV and its jth neighbor. ϕ_j is defined as $e^{-\theta_0 |d_j - d_i|}$, $|d_j - d_i|$ is the distance between the ith UAV and its jth neighbor, θ_0 is a positive adjustable parameter (here we let $\theta_0 = 0.002$) [38].

TABLE I
COMPARISON OF SIX ALGORITHMS

Algorithm	Test Statistic	Information Overhead	Time Complexity
3DNCS	$E_i(k)$	1	$O(m)$
3DCS	$\sum_{i=1}^{\lvert N\rvert}\omega_i E_i(k)$	$\lvert N\rvert$	$O(n)+O(m)$
3DSTS	$\sum_{j\in S}\rho_j\sum_{k=t-l+1}^{t}\omega_k E_j(k)$	$\lvert S\rvert l$	$O(n^2)+O(m)$
DF-3DSTS	$\sum_{j\in S}\rho_j\left[\sum_{j'\in S_j}\rho_{j'}\sum_{k=t-l+1}^{t}\omega_k E_{j'}(k)\right]$	$\sum_{j'\in S_j}\lvert S_{j'}\rvert l+\lvert S\rvert$	$O(2n^2)+O(m)$
TGSS	$\sum_{j\in S_{global}}\rho_j\sum_{k=t-l+1}^{t}\omega_k E_j(k)$	$\lvert N\rvert l$	$O(n^2)+O(m)$
DF-TGSS	$\sum_{j\in S_{global}}\rho_j\left[\sum_{j'\in S_j}\rho_{j'}\sum_{k=t-l+1}^{t}\omega_k E_{j'}(k)\right]$	$\sum_{j'\in S_j}\lvert S_{j'}\rvert l+\lvert N\rvert$	$O(2n^2)+O(m)$

Therefore, we get a 3DSTS fusion result obtained at the ith UAV,

$$T_{i,3DSTS}(t)=\sum_{j\in S}\rho_j\sum_{k=t-l+1}^{t}\omega_k E_j(k)\underset{O_o}{\overset{O_1}{\gtrless}}\lambda, i=1,\ldots,|N|, \tag{27}$$

B. 3DSTS Performance Analysis

According to (27), the distribution of the 3DSTS test statistic follows

$$E_{3DSTS}\sim\begin{cases}\mathcal{N}(\mu_{3DSTS,0},{\sigma_{3DSTS,0}}^2), & H_0\\ \mathcal{N}(\mu_{3DSTS,1}(r_i),{\sigma_{3DSTS,1}}^2(r_i)), & H_1\end{cases} \tag{28}$$

where

$$\begin{cases}\mu_{3DSTS,0}=\sum_{j\in S}\rho_j\sum_{k=1}^{t-l+1}\omega_k{\sigma_n}^2,\\ {\sigma_{3DSTS,0}}^2=\sum_{j\in S}\rho_j^2\sum_{k=t-l+1}^{t}2\omega_k^2{\sigma_n}^4/M,\\ \mu_{3DSTS,1}(r_i)=\sum_{j\in S}\rho_j\sum_{k=t-l+1}^{t}(1+\gamma_j)\omega_k{\sigma_n}^2,\\ {\sigma_{3DSTS,1}}^2(r_i)=\sum_{j\in S}\rho_j^2\sum_{k=t-l+1}^{t}\omega_k^2(1+2\gamma_j){\sigma_0}^2,\end{cases} \tag{29}$$

$\gamma_i=P_i(r_i)/{\sigma_n}^2$ represents the received signal to noise ratio (SNR) of the ith UAV.

Therefore, we obtain the spatial-temporal false alarm probability and detection probability of single UAV and whole network for the 3DSTS scheme.

$$P_{f,i}^{ST}(k)=\begin{cases}P_{f,i}^{T_0}(k), & 0\le r_i\le R_p,\\ (1-P_l)P_{f,i}^{T_0}(k)+P_lP_{d,i}^{T_l}(k), & R_p\le r_i\le R_s,\end{cases}$$

$$=\begin{cases}Q\left(\frac{\lambda-\mu_{3DSTS,0}}{\sigma_{3DSTS,0}}\right), & 0\le r_i\le R_p,\\ (1-P_l)Q\left(\frac{\lambda-\mu_{3DSTS,0}}{\sigma_{3DSTS,0}}\right)\\ \quad+P_lQ\left(\frac{\lambda-\mu_{3DSTS,1}(r_i)}{\sigma_{3DSTS,1}(r_i)}\right), & R_p\le r_i\le R_s,\end{cases} \tag{30}$$

$$P_{d,i}^{ST}(k)=P_{d,i}^{T_l}(k), \quad 0\le r_i\le R_p,$$
$$=Q\left(\frac{\lambda-\mu_{3DSTS,1}(r_i)}{\sigma_{3DSTS,1}(r_i)}\right), \quad 0\le r_i\le R_p, \tag{31}$$

$$P_{f,net}^{ST}=\frac{1}{|N|}\left\{\sum_{i\in N_{in}}Q\left(\frac{\lambda-\mu_{3DSTS,0}}{\sigma_{3DSTS,0}}\right)+\sum_{i\in N_{out}}\left[(1-P_l)Q\left(\frac{\lambda-\mu_{3DSTS,0}}{\sigma_{3DSTS,0}}\right)+P_lQ\left(\frac{\lambda-\mu_{3DSTS,1}(r_i)}{\sigma_{3DSTS,1}(r_i)}\right)\right]\right\}, \tag{32}$$

$$P_{d,net}^{ST}=\frac{1}{|N_{in}|}\sum_{i\in N_{in}}Q\left(\frac{\lambda-\mu_{3DSTS,1}(r_i)}{\sigma_{3DSTS,1}(r_i)}\right), \tag{33}$$

C. 3DSTS Algorithm Improvement

Based on the above 3DSTS scheme, we firstly propose two improved algorithms. We name them as double fusion 3D spatial-temporal sensing (DF-3DSTS) and temporal and global spatial sensing (TGSS), respectively.

In the DF-3DSTS scheme, we expend the 3DSTS from the test statistic itself. As the equation (25) shown, 3DSTS fuses the sensing results of the ith UAV and its neighbor UAVs in the same fusing sphere. Here the sensing result $\hat{T}_i(t)$ in (25) is merely from a single UAV, which does not take the correlation between the neighbor UAVs in the fusion sphere and their own secondary neighbor UAVs into consideration. Therefore, except the primary fusion of the ith UAV and its neighbor UAVs, we execute secondary fusion on the neighbor UAVs. That is, the sensing result of a neighbor UAV is also fused by exchanging information with the secondary neighbor UAVs in its secondary fusion sphere. Mathematically, we obtain the DF-3DSTS test statistic compared to (27),

$$T_{i,DF-3DSTS}(t)=\sum_{j\in S}\rho_j\left[\sum_{j'\in S_j}\rho_{j'}\sum_{k=t-l+1}^{t}\omega_k E_{j'}(k)\right], i=1,\ldots,|N|, \tag{34}$$

where S_j is the secondary fusion sphere of the jth neighbor UAV in the primary fusion sphere. $\rho_{j'}$ is the normalized spatial correlation weight coefficient of the j'th secondary neighbor UAV in S_j. $E_{j'}(k)$ is the sensing result of the j'th secondary neighbor UAV in the kth sensing period.

On the other hand, the TGSS scheme focuses on the global fusion of the ith UAV and its neighbor UAVs. That is, we include

all the UAVs in the primary fusion sphere so that the ith UAV fuses its sensing result with all the UAVs or the radius R_g is sufficiently large in other words. Therefore, we obtain the TGSS test statistic compared to (27),

$$T_{i,TGSS}(t) = \sum_{j \in S_{global}} \rho_j \sum_{k=t-l+1}^{t} \omega_k E_j(k), i = 1, \ldots, |N|, \tag{35}$$

where S_{global} is the UAV set which includes all UAVs.

These two algorithms improve the 3DSTS algorithm from two different perspectives. One focuses on the information each neighbor UAV uses in the primary fusion, and the other focuses on the number of neighbor UAVs participating in the primary fusion. Therefore, if we combine them together, we should obtain even better detection performance. Here we name this scheme as double fusion temporal and global spatial sensing (DF-TGSS), and easily we have its test statistic,

$$T_{i,DF-TGSS}(t) = \sum_{j \in S_{global}} \rho_j \left[\sum_{j' \in S_j} \rho_{j'} \sum_{k=t-l+1}^{t} \omega_k E_{j'}(k) \right], i = 1, \ldots, |N|, \tag{36}$$

In conclusion, we summarize the above six 3D spectrum sensing algorithms in Table I. We measure the information overhead of each algorithm by the amount of sensing results used in its test statistic. $|\cdot|$ denotes the size of the UAV set. Comparison of time complexity is also presented in the table, where m represents the length of the ergodic interval when solving the decision threshold λ in our algorithms, and n is the length of the input data. Simulations show the three improved algorithms gain better detection performance than the 3DSTS algorithm which will be presented in Section VI.

V. Sensing Based Power Control Scheme

In Section II, we have replaced the TV tower protected range R_{pp} with its transmission range R_p, and analyzed the composite spatial-temporal hypothesis testing problem. The *grey layer* is merged into the *white layer* which facilitates the analysis of the composite hypothesis testing problem and effectively improves the spectrum utilization. In this section, we will study the power control issue in 3D spectrum-heterogeneous networks. We will decide how much transmission power the UAV uses at different locations in the network.

As shown in Fig. 6, each UAV has a decision on the working state of TV Tower. UAV inside transmission range R_p declares O_1, UAV outside transmission range R_p declares O_0. Therefore, if the decision result is O_1, then no transmission for the UAV will be allowed; if the decision result is O_0, then the UAV further check its neighbor's decision results. In order to distinguish whether the UAV is in the *grey* or *white layer* with the help of neighbor UAVs, we let the protected range R_{pp} of TV tower minus the transmission range R_p equal the radius of the fusion sphere R_g. In this way, when the UAV is outside R_{pp}, all its neighbor UAVs in the fusion sphere declare O_0, which means the UAV can transmit peak power; when the UAV is inside R_{pp},

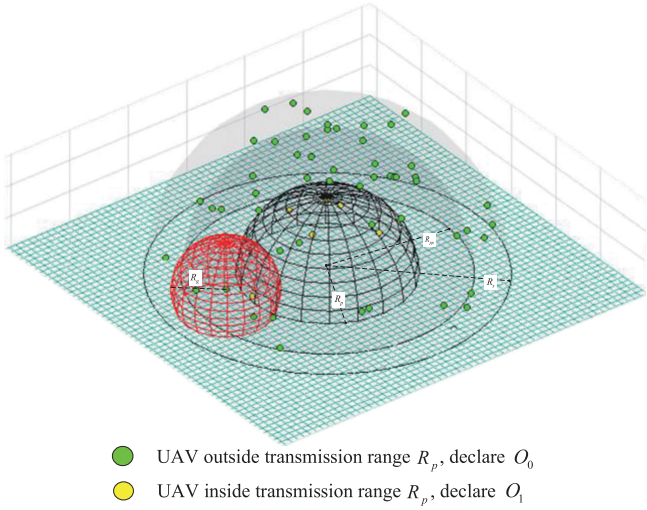

Fig. 6. 3DSTS based power control scheme. UAV in the *black layer* declares O_0, UAV in the *grey layer* and *black layer* declares O_1. R_g is the the radius of the fusion sphere and also the range of *grey layer*.

some neighbor UAVs declare O_0, some declare O_1, in this case we execute power control. As a result, the ideal 3D *black-grey-white* (Ideal 3D BGW) power control follows

$$\Pi_{peak,i}^{BGW} = \begin{cases} 0, & r_i \le R_p, H_1, \\ I_{th}(r_i - R_p)^n, & R_p < r_i \le R_{pp}, H_1, \\ \Pi_{peak}, & R_{pp} < r_i \le R_s, H_1, \\ \Pi_{peak}, & H_0, \end{cases} \tag{37}$$

where I_{th} is the interference constraint at the edge of the TV tower transmission range. Π_{peak} is the peak power a UAV can transmit. n is the path-loss exponent.

Specifically, according to the definition of constraint power $I_{th}(r_i - R_p)^n$ in the *grey layer*, we have

$$I_{th}(r_i - R_p)^n = I_{th} {R_g}^n = \Pi_{peak}, \tag{38}$$

thus we obtain the relationship between the peak power Π_{peak} and the interference constraint I_{th}.

To simplify the above Ideal 3D BGW power control scheme to ideal black-white (Ideal 3D BW) power control, we obtain the traditional black-white spatial opportunity in terms of protected range R_{pp},

$$\Pi_{peak,i}^{BW} = \begin{cases} 0, & r_i \le R_{pp}, H_1, \\ \Pi_{peak}, & R_{pp} < r_i \le R_s, H_1, \\ \Pi_{peak}, & H_0. \end{cases} \tag{39}$$

However, the above two power control schemes work out on the basis of the prior location information of the TV tower. If the location information is not available, we make an estimation as follows,

$$\begin{aligned} \Pi_{peak} &= I_{th}(r_i - R_p)^n = I_{th} {d_i}^n \\ &= \frac{1}{2}(I_{th} {d_{i,max}}^n + I_{th} {d_{i,min}}^n), \end{aligned} \tag{40}$$

where $d_{i,min}$ denotes the distance between the ith UAV and its nearest neighbor that declares O_1. $d_{i,max}$ denotes the distance between the ith UAV and its furthest neighbor, which declares

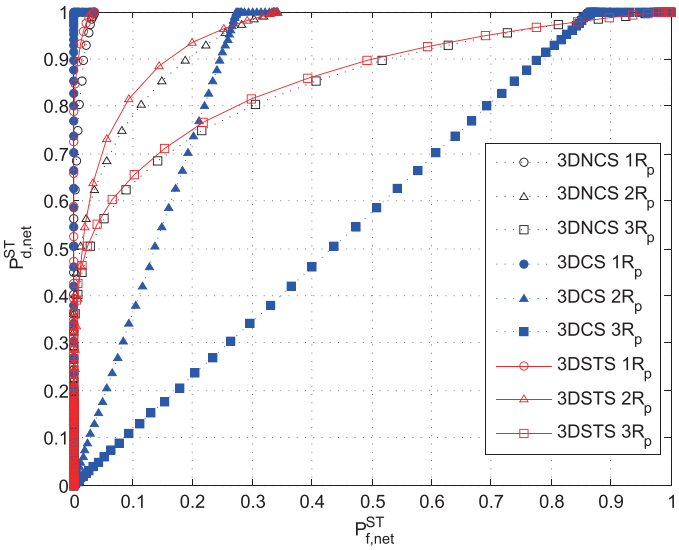

Fig. 7. Detection performance comparisons of 3DSTS and benchmark schemes in 3D spectrum-heterogeneous environments ($P_1 = 0.9$, $\rho = 0.2$).

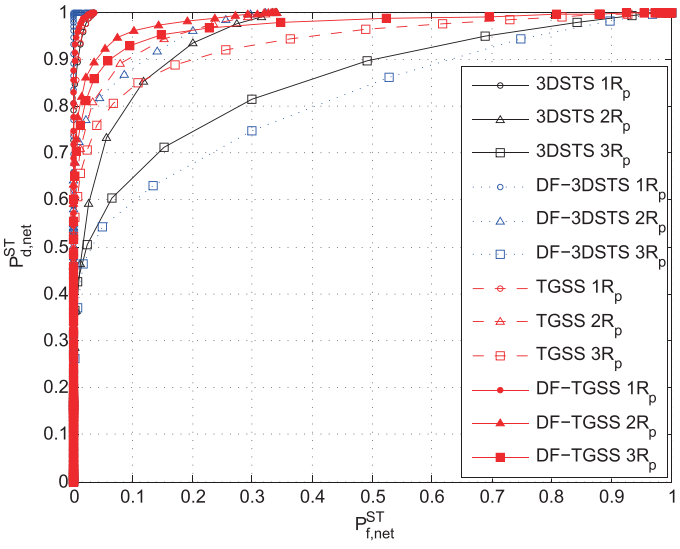

Fig. 8. Detection performance comparisons of 3DSTS and the improved schemes in 3D spectrum-heterogeneous environments ($P_1 = 0.9$, $\rho = 0.2$).

O_0 and has a smaller distance than $d_{i,min}$. Therefore, we name this practical power control scheme as 3D spatial-temporal sensing *black-grey-white* (3DSTS BGW) power control compared to the Ideal 3D BGW. In the future work, more accurate algorithms will be investigated on the position estimation of primary user as references [39], [40] show.

VI. Performance Evaluation and Discussions

A. Simulation Setup

In this section, we simulate six spectrum sensing schemes in the 3D spectrum-heterogeneous networks. Parameters are set as follows, the sensing period T_p is 100 ms, and the spectrum sensing duration T_s is 10 ms. The bandwidth is 2 MHz, the transmission power of the TV tower is assumed to be 30 mW. The receiver noise spectral density is -174 dBm/Hz. The path-loss exponent is 4. The 3D Poisson distributed UAV density $\rho = 0.2/\text{km}^3$. The transmission range of TV tower is $R_p = 2.5$ km. The temporal and spatial fusion parameters τ_0 and θ_0 are set $\tau_0 = 2.5$ and $\theta_0 = 0.002$, respectively. The probability that the PU is in the working state is $P_1 = 0.9$, and its state transition rates are $\varepsilon = 9 \times 10^{-4}$ times/ms and $\mu = 1 \times 10^{-4}$ times/ms. The interference constraint I_{th} at the edge of the TV tower transmission region is -130 dBm.

B. Comparison of Detection Performance

1) Impact of R_s: Firstly, we compare the whole network detection performance of the benchmark 3DNCS and 3DCS with the 3DSTS scheme ($R_s = 1R_p, 2R_p, 3R_p$ and $P_1 = 0.9$, $\rho = 0.2$). We can see in Fig. 7 that when UAVs all locate inside R_p, which means they are in a homogeneous spectrum environment, the 3DCS is better than the 3DNCS and 3DSTS. But the 3DSTS is generally better than the 3DCS and 3DNCS in the practical 3D spectrum-heterogeneous environment. This shows us cooperation is not always effective, it can bring extra spatial false alarm probability when the UAVs locate outside of R_p. On the other hand, the good performance of the 3DSTS scheme tells us consideration of spatial and temporal correlations between sensing results will gain improvement on network detection performance.

Then we simulate the 3DSTS with its improved algorithms as shown in Fig. 8. We can see the DF-3DSTS gains better network detection performance than the 3DSTS when R_s is relatively small ($R_s = 1R_p$ or $2R_p$). However, the DF-3DSTS is inferior to the 3DSTS when $R_s = 3R_p$ mainly due to the more spatial false alarm introduced by more cooperation in double fusion.

The TGSS outperforms the 3DSTS at three different R_s. Compared to the DF-3DSTS, the TGSS is superior when R_s is large ($R_s = 3R_p$). When $R_s = 2R_p$, the TGSS is comparable as the DF-3DSTS, and when R_s is small ($R_s = 1R_p$) the TGSS is a bit inferior to the DF-3DSTS.

Undoubtedly, when we combine DF-3DSTS with TGSS, the DF-TGSS shows much better network detection performance than any other sensing schemes as the corresponding curves shown in Fig. 8. The DF-TGSS not only exploits the advantages of the DF-3DSTS and TGSS, but also overcomes their weakness, which indicates that it is the best scheme for choice in 3D spectrum-heterogeneous environment.

2) Impact of P_1: In Fig. 9, we study the impact of TV tower's working probability P_1 on the network detection performance in different schemes. We consider three different values $P_1 = 0.3, 0.6, 0.9$ ($R_s = 3R_p$, $\rho = 0.2$). Obviously, for all schemes, with lower P_1, the UAVs obtain better network detection performance. Because with the lower probability TV tower is ON, the fewer spatial false alarms occur. Moreover, the improved DF-TGSS and TGSS outperform other sensing schemes.

3) Impact of ρ: Furthermore, the impact of UAV density ρ is studied as shown in Fig. 10. We consider five different density values $\rho = 0.02, 0.1, 0.2, 1, 2$ ($P_1 = 0.9$, $R_s = 3R_p$) for the three improved algorithms. From the simulation, we can see that for each algorithm, the performance first decreases and then increases as ρ increases. Specifically, among the selected densities, the detection performance reaches the lowest when

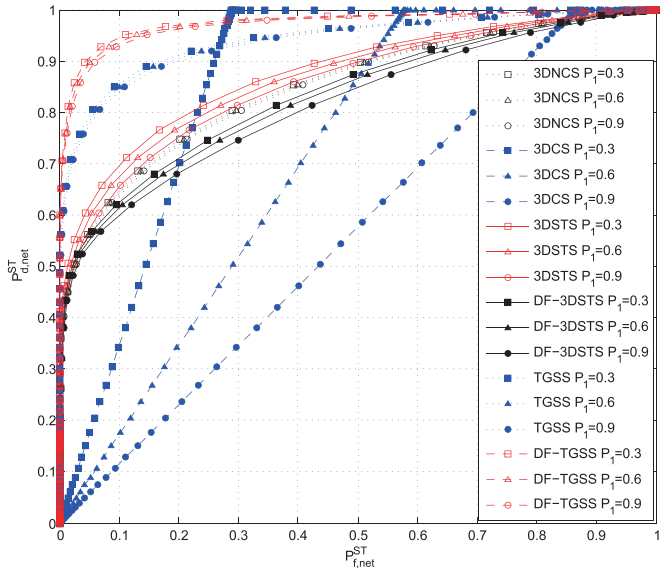

Fig. 9. Impact of P_1 on detection performance comparisons in 3D spectrum-heterogeneous environments ($R_s = 3R_p$, $\rho = 0.2$).

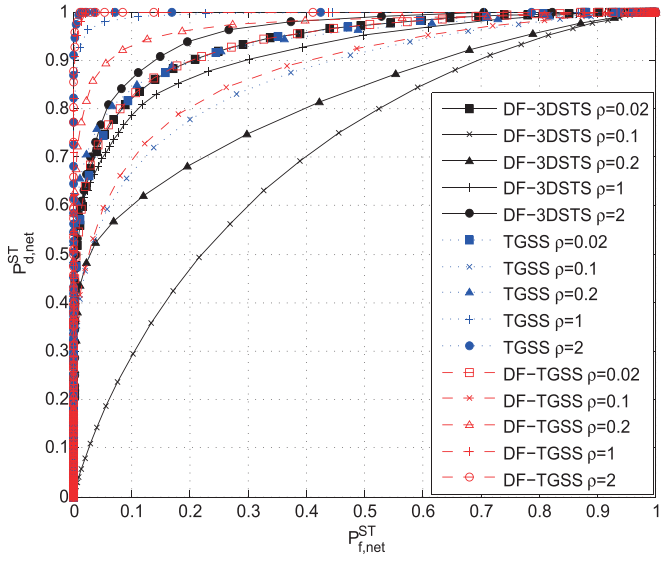

Fig. 10. Impact of ρ on detection performance comparisons in 3D spectrum-heterogeneous environments ($P_1 = 0.9$, $R_s = 3R_p$).

$\rho = 0.1$. Generally, the DF-TGSS and TGSS are superior to the DF-3DSTS which suffers a large performance fluctuation by changing ρ.

4) Air to Ground Channel vs. LOS Channel: In this part, we investigate the impact of channel model on the detection performance of spectrum sensing. Typically, the received signal composes of several components, including LOS (Line of Sight), strong reflected NLOS (Non-Line of Sight) and fading etc. Here we consider the air to ground channel as a combination of LOS and NLOS along with their occurrence probabilities and neglect the small scale fading [41], [42]. We define the total path loss L as:

$$L = P(LOS) \times L_{LOS} + P(NLOS) \times L_{NLOS}, \quad (41)$$

$$P(LOS) = \frac{1}{1 + \alpha \exp(-\beta[\frac{180}{\pi}\theta - \alpha])}, \quad (42)$$

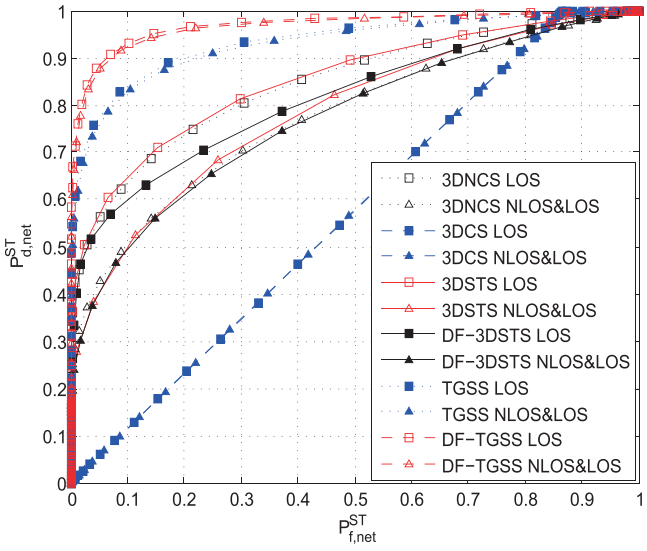

Fig. 11. Detection performance comparisons of LOS and NLOS&LOS channel ($P_1 = 0.9$, $R_s = 3R_p$, $\rho = 0.2$).

where $P(LOS)$ and $P(NLOS)$ are the occurrence probabilities of LOS and NLOS links, L_{LOS} and L_{NLOS} represent the corresponding path loss. The probability $P(LOS)$ is determined by α, β, θ, of which the parameters α, β are decided by the environment, the θ is the elevation angle of the UAV (here we let $\alpha = 9.6, \beta = 0.28$ [41]).

Obviously, from Fig. 11 we can see consideration of NLOS will decrease the network detection performance with different degrees. For 3DCS, it almost keeps the same performance. For 3DNCS, 3DSTS and DF-3DSTS, their performance attenuation is relatively close. Moreover, TGSS and DF-TGSS decrease much less than the others. These observations help us to choose the outperforming spectrum sensing method in different environments. That is, if the environmental conditions are bad, the channel propagation interference impacts greatly, then we can choose DF-TGSS for high network detection performance and low performance fluctuation, or TGSS with slightly lower performance but less computational cost. If the environmental interference is mild or our performance requirements are not very high, and we prefer fast detection, then we can choose 3DNCS and 3DSTS, or DF-3DSTS which sacrifices a little performance in exchange for slighter fluctuation.

C. Comparison of Network Averaged MICTP

Furthermore, power control is applied to the 3D spectrum-heterogeneous network according to Section V. We simulate the relationship between network average maximum interference constrained transmission power (MICTP) and the peak transmission power Π_{peak} as shown in Fig. 12. Some parameters are set as follows, $P_1 = 0.9$, $R_s = 3R_p$, $\rho = 0.2$, R_g ranges from 0 to $2R_p$. We compare three different schemes, Ideal 3D BGW, Ideal 3D BW and 3DSTS BGW. We can see the network averaged MICTP of the Ideal 3D BW first increases and then decreases with the increasing peak transmission power Π_{peak}. This is mainly because R_g is relatively small at the beginning, so the MICTP of the UAVs outside the R_{pp} gradually increases with Π_{peak}, but afterwards the number of UAVs outside the R_{pp}

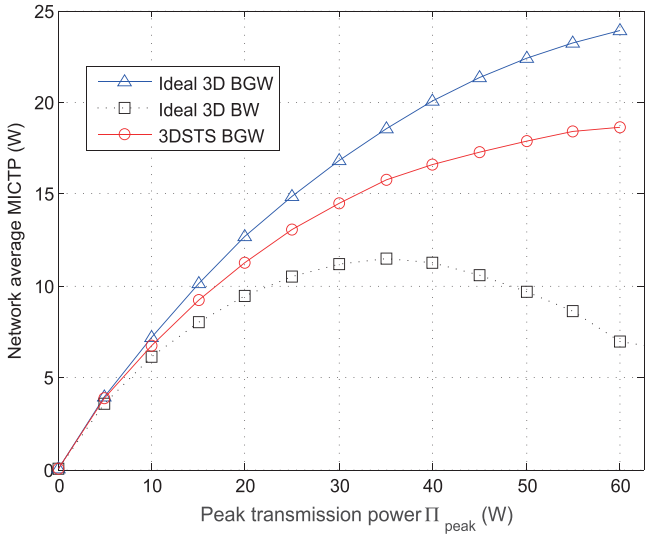

Fig. 12. Network average MICTP versus UAV peak transmission power Π_{peak}.

gradually decreases to a small amount, thus the space opportunity decreases. However, the network averaged MICTP of Ideal 3D BGW always increases with Π_{peak}, mainly because of the exploitation of spectrum opportunities in the *grey layer*. Lastly, the 3DSTS BGW is also monotonically increasing. But due to the approximation on $r_i - R_p$ in Eq.(40), it achieves a smaller network averaged MICTP than the Ideal 3D BGW scheme.

VII. Conclusion

In this paper, we investigate the issue of UAV-based 3D spectrum sensing in spectrum-heterogeneous networks. We firstly define the 3D spatial-temporal spectrum access opportunity based on UAVs who have location flexibility and also the requirement to opportunistically access the TV band. Then, we formulate the 3D spectrum-heterogeneous sensing model and derive the performance metrics. We propose a 3D spatial-temporal sensing (3DSTS) framework by effectively fusing the sensing results in a temporal fusion window and a spatial fusion sphere jointly. Compared to 3DNCS and 3DCS, it shows cooperation is not as effective as that in homogeneous environment, but exploitation of spatial and temporal correlations benefits the detection performance a lot. We further develop three improved versions of 3DSTS which achieve much better detection performance. Moreover, a sensing based power control scheme for *black-grey-white* network model is applied to improve the spectrum utilization. Impact of different parameters on the detection performance is also studied, thus we are able to choose the best sensing method in different spectrum environment. Further research will be conducted to investigate several issues including more accurate algorithms on the PU position estimation in the sensing based power control scheme and the optimal design of the temporal fusion window as well as the spatial fusion sphere. What's more, constraints of UAV-based sensing will also be taken into consideration, e.g., the battery constraints and irregular surveillance area etc. [43], [44].

References

[1] Z. Feng, C. Qiu, Z. Feng, Z. Wei, W. Li, and P. Zhang, "An effective approach to 5G: Wireless network virtualization," *IEEE Commun. Mag.*, vol. 53, no. 12, pp. 53–59, Dec. 2015.
[2] FCC, "Spectrum policy task force report," Washington, DC, USA, ET Docket 02-135, Nov. 2002.
[3] FCC, "Facilitating opportunities for flexible, efficient, and reliable spectrum use employing cognitive radio technologies," Washington, DC, USA, ET Docket 03-108, Dec. 2003.
[4] G. Ding, J. Wang, Q. Wu, Y.-D. Yao, F. Song, and T. A. Tsiftsis, "Cellular-base-station-assisted device-to-device communications in TV white space," *IEEE J. Sel. Areas Commun.*, vol. 34, no. 1, pp. 107–121, Jan. 2016.
[5] S. Haykin, "Cognitive radio: Brain-empowered wireless communications," *IEEE J. Sel. Areas Commun.*, vol. 23, no. 2, pp. 201–220, Feb. 2005.
[6] J. Mitola and G. Q. Maguire, "Cognitive radio: Making software radios more personal," *IEEE Pers. Commun.*, vol. 6, no. 4, pp. 13–18, Aug. 1999.
[7] B. Wang and K. R. Liu, "Advances in cognitive radio networks: A survey," *IEEE J. Sel. Topics Signal Process.*, vol. 5, no. 1, pp. 5–23, Feb. 2011.
[8] Y. Chen, G. Yu, Z. Zhang, H.-H. Chen, and P. Qiu, "On cognitive radio networks with opportunistic power control strategies in fading channels," *IEEE Trans. Wireless Commun.*, vol. 7, no. 7, pp. 2752–2761, Jul. 2008.
[9] Q. Zhao and B. M. Sadler, "A survey of dynamic spectrum access," *IEEE Signal Process. Mag.*, vol. 24, no. 3, pp. 79–89, Jun. 2007.
[10] Y. Xu, J. Wang, Q. Wu, A. Anpalagan, and Y.-D. Yao, "Opportunistic spectrum access in unknown dynamic environment: A game-theoretic stochastic learning solution," *IEEE Trans. Wireless Commun.*, vol. 11, no. 4, pp. 1380–1391, Feb. 2012.
[11] S. Geirhofer, L. Tong, and B. M. Sadler, "Cognitive radios for dynamic spectrum access-dynamic spectrum access in the time domain: Modeling and exploiting white space," *IEEE Commun. Mag.*, vol. 45, no. 5, pp. 66–72, May 2007.
[12] Z. Ji and K. R. Liu, "Cognitive radios for dynamic spectrum access-dynamic spectrum sharing: A game theoretical overview," *IEEE Commun. Mag.*, vol. 45, no. 5, pp. 88–94, May 2007.
[13] A. Ghasemi and E. S. Sousa, "Optimization of spectrum sensing for opportunistic spectrum access in cognitive radio networks," in *Proc. 4th IEEE Consum. Commun. Netw. Conf.*, Las Vegas, NV, USA, Jan. 2007, pp. 1022–1026.
[14] L. Zeng, X. Cheng, C. Wang, and X. Yin, "A 3D geometry-based stochastic channel model for UAV-MIMO channels," in *Proc. IEEE Wireless Commun. Netw. Conf.*, San Francisco, CA, USA, Mar. 2017, pp. 1–5.
[15] C. Zhang and W. Zhang, "Spectrum sharing for drone networks," *IEEE J. Sel. Areas Commun.*, vol. 35, no. 1, pp. 136–144, Jan. 2017.
[16] G. Ding, Q. Wu, L. Zhang, Y. Lin, T. A. Tsiftsis, and Y.-D. Yao, "An amateur drone surveillance system based on the cognitive Internet of Things," *IEEE Commun. Mag.*, vol. 56, no. 1, pp. 29–35, Jan. 2018.
[17] J. Ma, G. Zhao, and Y. Li, "Soft combination and detection for cooperative spectrum sensing in cognitive radio networks," *IEEE Trans. Wireless Commun.*, vol. 7, no. 11, pp. 4502–4507, Nov. 2008.
[18] Z. Quan, S. Cui, and A. H. Sayed, "Optimal linear cooperation for spectrum sensing in cognitive radio networks," *IEEE J. Sel. Topics Signal Process.*, vol. 2, no. 1, pp. 28–40, Feb. 2008.
[19] T. Yucek and H. Arslan, "A survey of spectrum sensing algorithms for cognitive radio applications," *IEEE Commun. Surveys Tuts.*, vol. 11, no. 1, pp. 116–130, Mar. 2009.
[20] D. Duan, L. Yang, and J. C. Principe, "Cooperative diversity of spectrum sensing for cognitive radio systems," *IEEE Trans. Signal Process.*, vol. 58, no. 6, pp. 3218–3227, Jun. 2010.
[21] E. Visotsky, S. Kuffner, and R. Peterson, "On collaborative detection of TV transmissions in support of dynamic spectrum sharing," in *Proc. 1st IEEE Int. Symp. New Frontiers Dyn. Spectr. Access Netw.*, Baltimore, MD, USA, Nov. 2005, pp. 338–345.
[22] I. F. Akyildiz, B. F. Lo, and R. Balakrishnan, "Cooperative spectrum sensing in cognitive radio networks: A survey," *Phys. Commun.*, vol. 4, no. 1, pp. 40–62, Mar. 2011.
[23] C. Liu, M. Li, and M.-L. Jin, "Blind energy-based detection for spatial spectrum sensing," *IEEE Wireless Commun. Lett.*, vol. 4, no. 1, pp. 98–101, Feb. 2015.
[24] D. M. S. Bhatti and H. Nam, "Spatial correlation based analysis of soft combination and user selection algorithm for cooperative spectrum sensing," *IET Commun.*, vol. 11, no. 1, pp. 39–44, Jan. 2017.

[25] B. L. Mark and A. O. Nasif, "Estimation of maximum interference-free power level for opportunistic spectrum access," *IEEE Trans. Wireless Commun.*, vol. 8, no. 5, pp. 2505–2513, May 2009.
[26] W. Han, J. Li, Q. Liu, and L. Zhao, "Spatial false alarms in cognitive radio," *IEEE Commun. Lett.*, vol. 15, no. 5, pp. 518–520, May 2011.
[27] S. M. Mishra, "Maximizing available spectrum for cognitive radios," Ph.D. Dissertation., Dept. Elect. Eng. Comput. Sci., Univ. of California Berkeley, Berkeley, CA, USA, 2009.
[28] A. Zaeemzadeh, M. Joneidi, N. Rahnavard, and G.-J. Qi, "Co-SpOT: Cooperative spectrum opportunity detection using Bayesian clustering in spectrum-heterogeneous cognitive radio networks," *IEEE Trans. Cogn. Commun. Netw.*, vol. 4, no. 2, pp. 206–219, Jun. 2018.
[29] H. Li, "Cooperative spectrum sensing via belief propagation in spectrum-heterogeneous cognitive radio systems," in *Proc. IEEE Wireless Commun. Netw. Conf.*, Sydney, NSW, Australia, Apr. 2010, pp. 1–6.
[30] P. Chen, Q. Zhang, J. Yu, Y. Zhang, and B. Cao, "Sensing-throughput tradeoff in joint spatial-temporal sensing based cognitive radio networks," in *Proc. IEEE/CIC Int. Conf. Commun. China*, Xi'an, China, Aug. 2013, pp. 727–732.
[31] T. Do and B. L. Mark, "Joint spatial-temporal spectrum sensing for cognitive radio networks," *IEEE Trans. Veh. Technol.*, vol. 59, no. 7, pp. 3480–3490, Sep. 2010.
[32] P.-H. Lee and P.-Y. Tsai, "Design and implementation of spatial-temporal spectrum sensing in cooperative cognitive radio sensor network," in *Proc. Int. SoC Des. Conf.*, Gyungju, South Korea, Nov. 2015, pp. 25–26.
[33] Q. Wu, G. Ding, J. Wang, and Y.-D. Yao, "Spatial-temporal opportunity detection for spectrum-heterogeneous cognitive radio networks: Two-dimensional sensing," *IEEE Trans. Wireless Commun.*, vol. 12, no. 2, pp. 516–526, Feb. 2013.
[34] R. Pasupathy, "Generating homogeneous Poisson processes," *Wiley Encyclopedia of Operations Research and Management Science*. Hoboken, NJ, USA: Wiley, Jan. 2010.
[35] J. Ma, G. Y. Li, and B. H. Juang, "Signal processing in cognitive radio," *Proc. IEEE*, vol. 97, no. 5, pp. 805–823, May 2009.
[36] H. Urkowitz, "Energy detection of unknown deterministic signals," *Proc. IEEE*, vol. 55, no. 4, pp. 523–531, Apr. 1967.
[37] Y.-C. Liang, Y. Zeng, E. C. Peh, and A. T. Hoang, "Sensing-throughput tradeoff for cognitive radio networks," *IEEE Trans. Wireless Commun.*, vol. 7, no. 4, pp. 1326–1337, Apr. 2008.
[38] M. Gudmundson, "Correlation model for shadow fading in mobile radio systems," *Electron. Lett.*, vol. 27, no. 23, pp. 2145–2146, Nov. 1991.
[39] X. Zhang, L. Xu, L. Xu, and D. Xu, "Direction of departure (DOD) and direction of arrival (DOA) estimation in MIMO radar with reduced-dimension MUSIC," *IEEE Commun. Lett.*, vol. 14, no. 12, pp. 1161–1163, Dec. 2010.
[40] F. Penna and D. Cabric, "Cooperative DOA-only localization of primary users in cognitive radio networks," *EURASIP J. Wireless Commun. Netw.*, vol. 2013, no. 1, pp. 1–14, Apr. 2013.
[41] M. Mozaffari, W. Saad, M. Bennis, and M. Debbah, "Drone small cells in the clouds: Design, deployment, and performance analysis," in *Proc. IEEE Global Commun. Conf.*, San Diego, CA, USA, Dec. 2015, pp. 1–6.
[42] Z. Han, A. L. Swindlehurst, and K. J. R. Liu, "Optimization of MANET connectivity via smart deployment/movement of unmanned air vehicles," *IEEE Trans. Veh. Technol.*, vol. 58, no. 7, pp. 3533–3546, Sep. 2009.
[43] Z. Zhou *et al.*, "When mobile crowd sensing meets UAV: Energy-efficient task assignment and route planning," *IEEE Trans. Commun.*, vol. 66, no. 11, pp. 5526–5538, Nov. 2018.
[44] Y. Yang, Z. Zheng, K. Bian, L. Song, and Z. Han, "Real-time profiling of fine-grained air quality index distribution using UAV sensing," *IEEE Internet Things J.*, vol. 5, no. 1, pp. 186–198, Feb. 2018.

Feng Shen received the B.S. degree in information engineering from the Nanjing University of Aeronautics and Astronautics, Nanjing, China, in 2017. He is currently working toward the M.S. degree with the College of Electronics and Information Engineering, Nanjing University of Aeronautics and Astronautics. His research interests include cognitive information theory, cognitive radio, signal processing, and wireless communications.

Guoru Ding (S'10–M'14–SM'16) received the B.S. degree (Hons.) in electrical engineering from Xidian University, Xian, China, in 2008, and the Ph.D. degree (Hons.) in communications and information systems from the College of Communications Engineering, Nanjing, China, in 2014. From 2014 to 2017, he was an Assistant Professor with the College of Communications Engineering and a Research Fellow with the National High Frequency Communications Research Center of China, Nanjing, China, where he is currently an Associate Professor. Since April 2015, he has been a Postdoctoral Research Associate with the National Mobile Communications Research Laboratory, Southeast University, Nanjing, China. His research interests include cognitive radio networks, massive multiple-input multiple-output, machine learning, and big data analytics over wireless networks.

He has served as a Guest Editor of the IEEE JOURNAL ON SELECTED AREAS IN COMMUNICATIONS (Special Issue on spectrum sharing and aggregation in future wireless networks). He is currently an Associate Editor of the *Journal of Communications and Information Networks*, the *KSII Transactions on Internet and Information Systems*, and the *AEU-International Journal of Electronics and Communications*. He has acted as Technical Program Committee Member for a number of international conferences, including the IEEE Global Communications Conference, the IEEE International Conference on Communications, and the IEEE Vehicular Technology Conference (VTC). He is a Voting Member of the IEEE 1900.6 Standard Association Working Group. He received the best paper awards from the EAI MLICOM 2016, the IEEE VTC 2014-Fall, and the IEEE WCSP 2009. He was also the recipient of the Alexander von Humboldt Fellowship in 2017 and the Excellent Doctoral Thesis Award of China Institute of Communications in 2016.

Zheng Wang received the B.S. degree in electronic and information engineering from the Nanjing University of Aeronautics and Astronautics, Nanjing, China, in 2009, the M.S. degree in communications from the University of Manchester, Manchester, U.K., in 2010, and the Ph.D degree in communication engineering from Imperial College London, London, U.K., in 2015.

From 2015 to 2016, he was a Research Associate at Imperial College London. From 2016 to 2017, he was a Senior Engineer with Radio Access Network R&D Division, Huawei Technologies Company. He is currently an Assistant Professor with the College of Electronics and Information Engineering, Nanjing University of Aeronautics and Astronautics. His current research interests include lattice methods for wireless communications, cognitive radio, and physical layer security.

Qihui Wu (SM'13) received the B.S. degree in communications engineering and the M.S. and Ph.D. degrees in communications and information systems from the Institute of Communications Engineering, Nanjing, China, in 1994, 1997, and 2000, respectively. From 2003 to 2005, he was a Postdoctoral Research Associate with Southeast University, Nanjing. From 2005 to 2007, he was an Associate Professor with the College of Communications Engineering, PLA University of Science and Technology, Nanjing, where he was a Full Professor from 2008 to 2016. Since May 2016, he has been a Full Professor with the College of Electronic and Information Engineering, Nanjing University of Aeronautics and Astronautics, Nanjing, China. From March 2011 to September 2011, he was an Advanced Visiting Scholar with the Stevens Institute of Technology, Hoboken, NJ, USA. His current research interests include the areas of wireless communications and statistical signal processing, with emphasis on system design of software defined radio, cognitive radio, and smart radio.